HHS Public Access

Author manuscript

Biomaterials. Author manuscript; available in PMC 2021 October 01.

Published in final edited form as:

Biomaterials. 2020 October ; 257: 120251. doi:10.1016/j.biomaterials.2020.120251.

Slow degrading poly(glycerol sebacate) derivatives improve vascular graft remodeling in a rat carotid artery interposition model

Jiayin Fu, **Xiaochu Ding**, **Chelsea E.T. Stowell**, **Yen-Lin Wu**, **Yadong Wang***

Nancy E. and Peter C. Meining School of Biomedical Engineering, Ithaca, NY 14853

Abstract

Porous synthetic grafts made of poly(glycerol sebacate) (PGS) can transform into autologous vascular conduits in vivo upon degradation of PGS. A long-held doctrine in tissue engineering is the necessity to match degradation of the scaffolds to tissue regeneration. Here, we tested the impact of degradation of PGS and its derivative in an interposition model of rat common carotid artery (CCA). Previous work indicates a complete degradation of PGS within approximately 2 weeks, likely at the fast end of the spectrum. Thus, the derivation of PGS focuses on delay degradation by conjugating the free hydroxy groups in PGS with a long chain carboxylic acid: palmitic acid, one of the most common lipid components. We evaluated two of the resultant palmitate-PGS (PPGS) in this study: one containing 9% palmitate (9-PPGS) and the other16% palmitate (16-PPGS). 16-PPGS grafts had the highest patency. Ultrasound imaging showed that the lumens of 16-PPGS grafts were similar to CCA and smaller than 9-PPGS and PGS grafts 12 weeks post-operation. Immunohistological and histological examination showed an endothelialized lumens in all three types of grafts within 4 weeks. Inflammatory responses to 16-PPGS grafts were limited to the adventitial space in contrast to a more diffusive infiltration in 9-PPGS and PGS grafts in week 4. Examination of calponin$^+$ and αSMA$^+$ cells revealed that 16-PPGS grafts remodeled into a distinctive bi-layered wall, while the walls of 9-PPGS grafts and PGS grafts only had one thick layer of smooth muscle-like cells. Correspondingly, the expression of collagen III and elastin displayed an identical layered structure in the remodeled 16-PPGS grafts, in contrast to a more spread distribution in 9-PPGS and PGS grafts. All the three types of grafts exhibited the same collagen content and burst pressure after 12 weeks of host remodeling. However, the compliance and elastin content of 16-PPGS grafts in week 12 were closest to those

* **Corresponding author:** yw839@cornell.edu .

We declare that we have no known competing financial interests or personal relationships that could have appeared to influence the work reported in this paper.

Credit Author Statement

Jiayin Fu: Investigation, Methodology, Formal analysis, Visualization, Writing - Original Draft, Writing - Review & Editing
Xiaochu Ding: Resources, Writing - Review & Editing
Chelsea E.T. Stowell: Methodology, Formal analysis
Yen-Lin Wu: Methodology
Yadong Wang: Conceptualization, Writing - Review & Editing, Supervision, Funding acquisition

of CCA. Overall, placing the degradation of PGS derived elastomer to a window of 4–12 weeks results in vascular conduits closer to arteries in a rat carotid artery interposition model over a 12-week observation period.

Keywords

degradation; poly(glycerol sebacate); vascular graft; artery; tissue engineering

1. Introduction

Coronary heart disease is still the leading cause of death in developed countries. The primary cause of coronary heart disease is the hardening and narrowing of coronary arteries, which reduces blood flow to heart muscles. For patients not suitable for stenting, coronary artery bypass grafting (CABG) is an alternative, which is a surgery that first harvests patients' own arteries or veins before using them as grafts to bypass the occluded coronary arteries and restore blood flow to the heart. However, this surgery is limited by availability of usable autologous grafts and inevitably causes donor site morbidity [1–4]. Conventional synthetic grafts, based on polyethylene terephthalate (Dacron) and expanded polytetrafluoroethylene (ePTFE), perform sufficiently well in large blood vessels [5, 6], but fail in small-diameter (<6 mm) vessels due to thrombosis and stenosis [7, 8]. Thus, synthetic grafts suitable for small arteries is an urgent and unmet need. Tissue engineering has the hope to develop truly useful small-diameter vascular grafts [9–12]. Yet, cell isolation, seeding and in vitro culture of tissue-engineered grafts are time-consuming and costly [13, 14].

A cell-free synthetic graft can transform into a vessel-like structure in situ by exploiting the host's inherent regeneration capacity. Bypassing cell harvesting and in vitro maturation procedures, the synthetic vascular grafts are more economical to produce and simpler to store and transport, facilitating potential adoption [15]. Decellularized vessels are acellular grafts derived from native vessels or *in vitro* bio-engineered vessels, where living cells are removed with extracellular matrixes (ECM) left behind [16]. The feasibility of this approach has been tested in large animals and clinic studies [16, 17]. However, these grafts are still expensive to produce and have low primary patency in the most recent clinical trial [18]. Vascular grafts made of biodegradable synthetic polymers, such as polyurethane and poly(ε-caprolactone) (PCL), have also been reported and show potentials as small-diameter vascular grafts in preclinical trials. However, fast degradation of polyurethane leads to graft dilation and limits its use in clinic [19–21], while chronic inflammation due to slow degrading PCL makes graft calcified easily, finally resulting in the dilation or thrombogenesis of the grafts [22, 23]. Natural protein polymer, such as silk, is an alternative to synthetic biodegradable polymers as materials for vascular grafts. Electrospun silk conduit has shown promises as a small diameter graft [24], but its long-term inflammatory responses and stability *in vivo* still need to be investigated.

In our previous studies, we have designed a composite synthetic vascular graft with the fast-degrading poly(glycerol sebacate) (PGS) as cores and slow-degrading PCL as sheaths [25]. The porous PGS core enables rapid cell infiltration and degradation [26, 27], while

the electrospun PCL sheath strengthens the graft and traps cells upon graft implantation *in vivo* [25]. Since most of the graft is made of PGS with only a thin layer of PCL, the graft is almost material-free after 3-month in rat abdominal aortas and well patent even 1 year post-implantation [28]. Such design of vascular grafts also works well in rat common carotid arteries (CCA) that has a smaller diameter and lower blood flow rate [29]. However, due to a fast degradation of PGS *in vivo*, upon the complete degradation of PGS cores, the graft walls are still not well structured. As a result, a trend of graft dilation could be observed occasionally.

We hypothesize that a more durable PGS derivatives could support smooth muscle cells (SMCs) for a longer period and enable more ECM deposition, thereby improving the overall performance of vascular grafts. To slow down the degradation of PGS, we conjugate free hydroxy groups in PGS with palmitic acid. The resultant polymer, palmitate modified PGS (PPGS), is more hydrophobic and degrades more slowly *in vitro* (Title: Control the mechanical properties and degradation profile of poly(glycerol sebacate) by substitution of the hydroxyl groups with palmitate, submitted to journal *Acta Biomaterialia*). We expect the same will be true *in vivo*, consistent with literature observation of decreased activity of enzymes on a hydrophobic surface [30–32]. For a proof of concept, we fabricated our vascular grafts using PPGS as new core materials and implant the grafts into rat carotid arteries to compare their performances with previous PGS grafts.

2. Method

2.1 Vascular graft fabrication

Vascular grafts were fabricated as described previously [29]. Ground salts (25–32 μm in size) were first packed into a tubular shape with a stainless-steel shaft (0.8 mm in diameter) as a mandrel and a PTFE tube (1.58 mm in diameter and 20 mm in length) as an outer sheath. After fusion of the salts, salt tubes were vacuum dried overnight at room temperature. 20% (w/v in tetrahydrofuran) Regenerez® Poly(glycerol sebacate) Resin (PGS, Secant Group), PPGS containing 9% palmitate (9-PPGS) or PPGS containing 16% palmitate (16-PPGS) was then added into the salt tubes in a mass ratio of salt : polymer=3 : 1, which were then crosslinked at 150°C in high vacuum for 24 hours. 14% (w/v in 2,2,2-trifluoroethanol) polycaprolactone (PCL, average Mn 80,000, Sigma-Aldrich) was electrospun onto the PGS-, 9-PPGS-, or 16-PPGS-salt tubes. The thickness of the PCL sheath was in a range of 20–25 μm. Following the electrospinning, the coated PGS-, 9-PPGS-, or 16-PPGS-PCL-salt tubes were soaked into deionized (DI) water for 72 hours with DI water changed every 24 hours to remove the salts. Finally, vascular grafts were lyophilized to remove the water. The three different types of vascular grafts were named as PGS, 9-PPGS and 16-PPGS, respectively. Prior to *in vivo* implantation, the grafts were sterilized with ethylene oxide (Andersen Products) and soaked into 180 units/mL (in saline solution) heparin overnight.

2.2 Characterization of the fabricated vascular grafts

The macro-structures of the fabricated vascular grafts were observed with a stereoscopic microscope (SMZ-745T, Nikon). The micro-structures of the fabricated vascular grafts were

observed under a field emission scanning electron microscope (FESEM, Mira3, Tescan). Samples were cut into 3 mm-long segments and sputter-coated prior to imaging. Lumen diameter and thickness of porous polymer layers and PCL sheaths were measured with the ImageJ software. 5 different samples (n=5) for each group were measured. Nano-scale X-ray computed tomography (Nano-CT, Xradia XRM CT instrument) scanning were used to view micro-structures of the grafts in three dimensions (3D). Samples (1.5 mm in length) were scanned at a resolution of 3.06 μm per pixel and 3D images were reconstructed with the software Avizo 2.0.

To evaluate cross-sections of the grafts, samples were soaked in 30% sucrose solution at 4°C for 24 hours. The grafts were then embedded vertically into the optimal cutting temperature compound (OCT, Sakura Finetek, USA), snap-frozen at −80°C, and cryosectioned at 10 μm thickness. The cut samples were directly observed with an inverted microscope (Eclipse Ti2, Nikon, Japan) in brightfield or under polarized light. Because sections of pure grafts fell off from slides when they went through a standard staining procedure, the implanted grafts were explanted for sectioning and staining just 24 hours post-implantation when the structures of the grafts were still intact. The explanted vascular grafts were rinsed with heparinized saline solution and soaked in 30% sucrose solution at 4°C for 24 hours. The vascular grafts were then embedded vertically into the OCT, snap-frozen at −80°C, and cryosectioned at 10 μm thickness. The slides were processed by the histology laboratory of Animal Health Diagnostic Center in Cornell University for hematoxylin and eosin (H&E) and Picro-sirius red staining. Images were taken with the inverted microscope in brightfield or under polarized light.

Mechanical properties of vascular grafts were measured with a material testing system (Instron, Model 5943) equipped with a 50 N static load cell. All samples were kept wet before testing and a uniaxial force was applied to the graft until the failure of graft cores. Strain and stress for each sample were recorded to acquire a stress-strain curve. The testing window was short enough that the samples were wet during the tests. Linear elastic modulus, ultimate tensile stress (UTS), and strain at break were calculated from the acquired stress-strain curve. Five different samples (n=5) were tested for each group.

The hydrophobicity of the fabricated vascular grafts was determined by weight change in water. Lyophilized vascular grafts were weighed and then immersed in deionized (DI) water for 48 hours. After 12, 24, and 48 hours, samples were taken out from water, gently tapped on wipers to remove surface waters and weighed again to measure the change in weight. The hydrophobicity was expressed as fold change in weight for each sample. Three different samples (n=3) from each group were used for hydrophobicity test.

The fabricated vascular grafts were immersed in sodium hydroxide (NaOH) solution to evaluate their degradation *in vitro*. Before alkaline solution treatment, the lyophilized samples were weighed to record their initial weight. Then, each graft was soaked in 5 mL 60 mM (in DI water, pH 12.87) NaOH (Sigma-Aldrich) and kept at 37°C for 5 hours. After 1, 3, and 5 hours, the samples were removed from the solution, washed with DI water, lyophilized and weighed again to record the weight change. The *in vitro* degradation was

expressed as percentage of weight loss for each sample. Three different specimens (n=3) were used for *in vitro* degradation test for each group at each time point.

Suture retention force of grafts was measured using the same material testing system as aforementioned. The samples for testing are approximately 5 mm in length. A single 9–0 Nylon suture (ARO Surgical) was pulled through the specimen 1 mm from the top edge. The suture and the non-sutured bottom of the sample were clamped in the upper and lower clamps of the testing machine, respectively. The suture was pulled at the rate of 50 mm/min. All the grafts were tested in wet at room temperature. Suture retention force was defined as the maximum force recorded before the suture was pulled out from each sample. Five different samples (n=5) were tested for each group.

2.3 Vascular graft implantation *in vivo*

All procedures were approved by the Institutional Animal Care and Use Committee (IACUC) at the Cornell University following NIH guidelines for the care and use of laboratory animals. A total of 39 male CD® (Sprague Dawley) IGS rats (strain code: 001, 10–12 weeks, body weight = 350–400 grams, n=39, Charles River Laboratories, Boston, MA) were used for vascular graft common carotid artery interposition. 14, 12, and 13 rats were used for 16-PPGS, 9-PPGS, and PGS vascular graft implantation respectively.

Rats were anesthetized by isoflurane inhalation (5% for induction, then 1.5% for maintenance). An incision at the midline of the neck was made and the left side muscles were retracted to expose the left common carotid artery. Blood flow of the common carotid artery was blocked with double microvascular clamps (Fine Science Tools, USA) and a 5-mm long segment of the common carotid artery was removed. A vascular graft was end-to-end anastomosed to the common carotid artery with 10–0 polyamide monofilament sutures (AROSurgical, Newport Beach, CA) by interrupted stitches. After the anastomosis, the microvascular clamps were removed from the common carotid artery to recover the blood flow. The surgical incision was closed with 3–0 absorbable sutures (Ethicon). No anticoagulation or antiplatelet treatments were administrated pre- and post-operatively. Analgesic (Buprenex, 0.05 mg/kg) were given once before the surgery and every 8 hours for 48 hours after the surgery.

2.4 Patency monitoring and performance evaluation with ultrasonography

VisualSonics Vevo-2100 High Resolution Ultrasound was used to monitor the inner diameter and the blood flow of the implanted vascular grafts on week 2, 4, 8 and 12 after implantation. Animals were anesthetized with 3% isoflurane in 1L/minute oxygen flow. The hair on the abdomen area was removed with hair removal cream and warm ultrasound gel was then applied to the skin before imaging. Ultrasound detector MS 400 was used for ultrasound imaging at a frequency of 30 MHz. B-mode, color doppler mode, and PW mode images along the long axis of the grafts were acquired. The patency and the inner diameter of the grafts was measured from the images of the color doppler mode. The peak flow rate of blood was directly read from the PW mode.

2.5 Histological and immunohistochemical analysis

4 and 12 weeks after the surgery, rats were anesthetized, and the implanted vascular grafts were exposed through a midline incision made on the neck and dissected out from surrounding tissues for analysis. The explanted vascular grafts were rinsed with heparinized saline solution, fixed in 4% paraformaldehyde (PFA, Electron Microscopy Sciences, USA) at 4°C for 1 hour, and soaked in 30% sucrose solution at 4°C for 24 hours. The vascular grafts were then embedded vertically into the optimal cutting temperature compound (OCT, Sakura Finetek, USA), snap-frozen at - 80°C, and cryosectioned at 10 μm thickness. The slides were sent to the histology laboratory of Animal Health Diagnostic Center in Cornell University for staining of H&E, Masson's trichrome, Verhoeff elastin, Picro-sirius red and Alizarin red, as well as immunohistochemical (IHC) staining of calponin and von willebrand factor (VWF). For IHC staining, the antibodies used are described in Table S1. Samples were visualized using bond polymer refine detection system (Leica, USA) and nuclei were counterstained with hematoxylin for 5 minutes. All histological images were captured with an inverted microscope (Eclipse Ti2, Nikon, Japan) in brightfield or under polarized light. H&E images from three different samples (n=3) for each group were used to quantify luminal area and wall thickness of grafts. Radius of grafts was first calculated through circumference of lumen and the luminal area was then calculated from the radius. The thickness of grafts was defined as the thickness of media layers. The thickness at six random spots for each graft was measured and the average thickness at those six spots were used to represent the thickness of that graft.

2.6 Immunofluorescence staining

Tissue sections (10-μm thick) were first blocked with 1% bovine serum albumin (BSA, Sigma-Aldrich) for 30 minutes at room temperature (RT) and then incubated with primary antibodies in 1% BSA at 4°C overnight. Following rinse with phosphate buffered saline (PBS, Fisher Scientific, USA), the samples were incubated with secondary antibodies in 1% BSA at RT for 1 hour. The antibodies used are described in Table S1. Nuclei were counterstained with 1μg/mL (w/v in DI water) 4', 6-diamidino-2-phenylindole (DAPI, Krackeler Scientific, USA). Tissue sections without a primary antibody incubation were used as negative controls. The stained samples were imaged with the inverted microscope. The area of positively stained cells and the area positive for DAPI were quantified with the software of ImageJ, respectively. Percentage of positively stained cells was calculated as a ratio between area of positively stained cells and area positive for DAPI staining. The percentage of positively stained cells was quantified through fluorescent images from three different samples (n=3) for each group.

2.7 Biochemical assays

Collagen contents of vascular grafts and the native common carotid arteries were measured using the Total Collagen Assay kit (BioVision, USA). Samples (3-mm in length) were minced finely, weighed to obtain wet weight, and then digested with 6M HCl at 120 °C for 3 hours. The soluble collagen content in the hydrolyzed samples was measured following the manufacturer's instructions and normalized to wet weight (μg/mg). For each group, three different samples (n=3) were measured.

Elastin contents of vascular grafts and the native common carotid arteries were measured using a Fastin™ Elastin Assay (Biocolor, UK). Samples (3-mm in length) were minced finely, weighed to obtain wet weight, and then digested with 0.25M oxalic acid at 100 °C for two 1 hour-cycles. After this, the soluble elastin content in the hydrolyzed samples was measured following the manufacturer's instructions and normalized to wet weight (μg/mg). For each group, three different samples (n=3) were measured.

2.8 Mechanical test

Circumferential mechanical properties of the explanted grafts were measured using a custom-designed inflation testing device. Entire segments of the explants were mounted on the device by suturing them on two 25G parallel needles. One end of the device was connected to a syringe pump that infused PBS at a rate of 60 μL/min and the other end was connected to a pressure monitor (Living Systems, USA) to record the luminal pressure. The change of outer diameters of the explants as a response to the pressure increase were recorded using a LS-7601 laser micrometer. All data were recorded using a data acquisition system (PowerLab 8/30, ADInstruments, Colorado Springs, CO) and the associated software LabChart 7.0. According to the obtained recorded stress-stretch curve, high-strain and modulus compliance were calculated, respectively. The high-strain modulus was calculated by fitting a line to the high strain region of the stress-stretch curve. The compliance (%/100 mmHg) was calculated using following equation and expressed as percent diameter change per 100 mmHg.

$$C = \frac{\frac{D_{high} - D_{low}}{D_{low}}}{P_{high} - P_{low}} \times 10,000$$

The burst pressure of the explanted grafts was measured by continued infusion of PBS at a rate of 5 mL/min until the grafts burst using the same apparatus with a pressure transducer of a higher range (PX309–100G5V, Omega Engineering Inc., Stamford, CT).

2.9 Statistical analysis

All data was presented as mean ± standard deviation. Each assay had at least three replicates and repeated 3 times independently. One-way ANOVA followed by Tukey's post-hoc test or two-tailed Student-t test was used to analyze the statistical significance. $P < 0.05$ was considered as statistically significant.

3. Results

3.1 Physical properties of the fabricated vascular grafts

In our previous study, we designed PPGS with appropriate contents of palmitate functionalities to make the elastomer softer with enhanced elasticity and at the same time increase hydrophobicity [33]. Compared to PGS, the PPGS with 9 and 16 mol.% of palmitate pendants reduced the elastic modulus from 838 ± 55 kPa to 441 ± 26 kPa and 333 ± 21 kPa, respectively. On the other hand, water contact angles of 9-PPGS and 16-PPGS

significantly increased from 66.3 ± 1.2° (PGS control) to 72.0 ± 1.8° and 84.8 ± 1.6°, demonstrating a proportional increase in hydrophobicity [33]. Both the 9-PPGS and 16-PPGS elastomers demonstrated a sustained release of palmitates over time (Supplementary Fig. 1). Such release kinetics indicates that the palmitate pendants are immobilized on the polymer backbone and slowly cleaved from the elastomer networks upon degradation. In addition, both 9-PPGS and 16-PPGS had a similar cytocompatibility to the PGS control as evaluated by cell viability and metabolic activity assays (Supplementary Fig. 2a). The increase in hydrophobicity of both 9-PPGS and 16-PPGS did not affect attachment, spread and morphologies of human umbilical vein endothelial cells (HUVECs), although a slight decrease in cell density was observed (Supplementary Fig. 2b–e).

In this study, we further explored the effects of 9-PPGS and 16-PPGS on graft remodeling in a rat carotid artery interposition model. Three different types of vascular grafts were made with the same design of a composite structure: an inner layer of porous polymer core and an outer layer of fibrous PCL sheath. Because all these vascular grafts were fabricated using the same mold, they had the same inner and outer diameter. The inner diameter of the grafts was 642.72 ± 17.04 μm, with a 341.14 ± 31.58 μm thick elastomer core and a 23.69 ± 4.33 μm thick PCL sheath. Nano-CT showed a highly porous core of the graft, while PCL sheath was invisible through the scanning (Fig. 1a). SEM examination showed the same porous core and a layer of dense electrospun PCL sheath (Fig. 1b). The unstained grafts showed a porous polymer core and a PCL sheath in a cross-sectional view. In addition, under polarized light, both core and sheath polymers showed distinct birefringence (Supplementary Fig. 3). For the grafts explanted 24 hours post-operation, core and sheath were thoroughly infiltrated with red blood cells but the structures of the grafts remained the same as the grafts before implantation (Supplementary Fig. 4). These characteristics of the grafts are consistent with our previously reported grafts for rat common carotid artery interposition [29].

The three types of the grafts showed a different hydrophobicity due to different core materials. PGS grafts were the most hydrophilic, with a 2-fold increase in weight after soaking 48 hours in water. In contrast, 9-PPGS and 16-PPGS grafts were more hydrophobic with their weight increasing to 1.3-fold (Fig. 1c). *In vitro* degradation of the different grafts was consistent with the observed hydrophobicity (Fig. 1d). 16-PPGS and 9-PPGS grafts lost approximately 10% and 15% of their initial weight 5 hours after NaOH treatment, respectively. PGS grafts showed a quick and significant weight loss of 95% after the same period of alkaline treatment.

Suture retention forces were the same in the different types of grafts (Fig. 1e). This is because suture retention force is mainly attributed to the PCL sheath [25], which was consistent among the different types of grafts. However, mechanical test showed a significant difference among them in stress-strain behavior (Fig.1f-i). Representative stress-strain curves showed that PGS grafts had a higher stress than the other two types of grafts in a stain from 20% to 60%, while 16-PPGS grafts displayed the lowest stress in the same range of strain (Fig.1f). In addition, both elastic modulus and UTS decreased with an increase of palmitate composition in PGS, whereas tensile strain at break showed a reverse trend (Fig.1g–i). These results indicate that palmitate modification renders PGS softer.

3.2 Vascular graft patency and performance after *in vivo* implantation

We implanted three different types of the grafts into the left common carotid arteries of 39 rats. To evaluate the patency of these grafts, blood flow in the left common carotid arteries of all the rats was monitored with ultrasound in week 2 and 4. In week 2, the overall patency for 16-PPGS, 9-PPGS and PGS group was 92.8% (13 out of 14 rats), 75% (9 out of 12 rats) and 69.2% (9 out of 13 rats), respectively. As there was no more graft obstruction after week 2, the overall patency in week 4 was the same as that of week 2 (Table 1).

To evaluate the performance of the vascular grafts *in vivo*, we continued to monitor the blood flow in the left common carotid arteries with the unoperated right side as a control every 4 weeks until week 12 (Fig. 2). From week 4 to 12, ultrasound images showed that there were backflows (red color, arrow heads, Fig. 2a) at anastomosis sites for both PGS and 9-PPGS groups, which indicates a dilation of the grafts that caused a relative narrowing to distal native common carotid arteries at the anastomosis sites in PGS and 9-PPGS grafts. The 16-PPGS group only showed a minimal backflow. Besides, distortion of the lumens could be observed in PGS and 9-PPGS groups (arrows, Fig. 2a), whereas 16-PPGS grafts showed a consistent and smooth lumen. Quantification of inner diameter of graft lumens showed that all grafts were larger than the native carotid arteries and the 16-PPGS grafts had a diameter closer to that of the native carotid arteries and stayed more consistent from week 4 to week 12. On the other hand, the inner diameter of 9-PGS and PGS grafts showed a trend of dilation and PGS grafts dilated even more than 9-PPGS grafts (Fig. 2c). There was no significant difference in the inner diameter between 9-PGS and PGS groups in week 4 and week 8, but the inner diameter of PGS grafts were significantly bigger than 9-PPGS grafts in week 8 and 12. Peak flow rate (as indicated by distance between two parallel dash lines in PW images of Fig. 2a) quantification showed that the flow rate decreased for all the three groups with the time of implantation (Fig. 2d). There was significant difference in flow rate between different groups in week 2 and the flow rate of 16-PPGS and 9-PPGS grafts was significantly higher than that of PGS grafts in week 8.

Macroscopic views of the different vascular grafts at time of implantation showed that 16-PPGS grafts had a non-homogeneous blood infiltration of the wall as compared to 9-PPGS and PGS grafts (Fig. 2b). It is probably caused by the higher hydrophobicity of 16-PPGS than 9-PPGS and PGS. Compared to less hydrophobic 9-PPGS and PGS grafts, 16-PPGS grafts did not submerge easily during the heparin solution treatment prior to graft implantation. With the time of graft remodeling *in vivo*, the difference between the synthetic grafts and the native arteries became minimal and could be identified only by suture materials (arrow heads in Fig. 2b). However, when explanted on week 12, 16-PPGS grafts were thinner and more reddish as compared to 9-PPGS and PGS grafts, suggesting a better remodeling for 16-PPGS grafts (Fig. 2b). Taken together, the 16-PPGS grafts had the best patency and performance *in vivo* among the three different types of grafts.

3.3 Histomorphometry assessments

To evaluate morphological differences between three different types of vascular grafts, mid-segments of the explanted grafts were cryo-sectioned and stained with H&E. PCL sheaths under polarized light showed a specific birefringence before implantation or 24

hours post-operation (Supplementary Fig. 3&4). The PCL sheaths still could be observed in H&E staining of 4-week and 12-week samples under polarized light (Fig. 3b). Demarcated by PCL sheaths, there were two distinctive layers for the vascular wall of 16-PPGS grafts in week 4: an inner layer and an outer layer. However, there was only one layer for 9-PPGS and PGS grafts. Closely examining the inner layer of unstained 16-PPGS graft samples in week 4, a small patch of material residuals that showed a darker color in brightfield images and a specific birefringence under polarized light could be seen (Supplementary Fig. 5). All these results indicate that 16-PPGS degrades slower than 9-PPGS and PGS *in vivo*. PCL layers that had the specific birefringence under polarized light were not obvious in week 12, which is probably due to gradual degradation of PCL sheaths *in vivo*.

H&E staining in brightfield showed that the vascular wall of 16-PPGS grafts had an inner layer of cells that embedded in materials and an outer thin layer of SMC-like cells that surrounded the whole grafts (Fig. 4a). This morphological property of the grafts mimics the muscular middle layer (media) and outer layer (adventitia) of native arteries. However, for both 9-PPGS and PGS grafts, there was only one thick layer of SMC-like cells. After 12 weeks *in vivo*, the inner layers of the 16-PPGS grafts became thinner, whereas 9-PPGS and PGS grafts still had one thick layer of SMC-like cells (Fig. 3b and 4b). Because lumen of explanted grafts was shrunken and irregular in shape without blood perfusion, luminal area of the grafts was calculated using radius derived from circumference of each graft. Quantification of luminal areas showed a smaller lumen in 16-PPGS groups as compared to 9-PPGS and PGS groups in week 4 and the lumen of 16-PPGS was still significantly smaller than that of PGS grafts in week 12 (Fig. 4c). Quantification of graft wall thickness showed that the graft wall of 9-PPGS and PGS grafts was significantly thicker than that of 16-PPGS grafts in both week 4 and week 12 (Fig. 4d).

3.4 Inflammatory responses

To evaluate inflammation associated with the grafts and clarify types of macrophages that participated in vascular graft remodeling, CD11b, CD206 and inducible nitric oxide synthase (iNOS) were stained in the mid-sections of the grafts in week 4 and 12. CD11b is a marker for leukocyte adhesion and migration and it was positively stained only in the adventitial space of 16-PPGS grafts in week 4. However, for 9-PPGS and PGS grafts, the staining of CD11b was transmural (Fig. 5a), indicating a wide spread of inflammatory cells in these two types of grafts. $CD11b^+$ cells also showed a higher percentage within 9-PPGS and PGS grafts than 16-PPGS grafts (Fig. 5g). By 12 weeks, most inflammation responses in all the grafts were resolved (Fig. 5d).

Monocytes/macrophages that mediate tissue regeneration were also characterized in this study. CD206 is a marker indicative of anti-inflammatory and pro-regenerative macrophages (M2 macrophages), while iNOS is a marker for pro-inflammatory macrophages (M1 macrophages). Both CD206 and iNOS showed a transmural distribution in 9-PPGS and PGS grafts, but only limited in the adventitial space of 16-PPGS grafts in week 4 (Fig. 5b and c). In addition, although $CD206^+$ and $iNOS^+$ cells in 9-PPGS and PGS grafts were much higher than those in 16-PPGS grafts, the ratio of $iNOS^+$ cells / $CD206^+$ cells was significantly lower in 16-PPGS grafts (Fig. 5h–j). These results indicate that both M1 and

M2 macrophages are involved in graft remodeling and a lower M1/M2 in 16-PPGS grafts suggests a superior micro-environment for vascular regeneration in 16-PPGS grafts than those in 9-PPGS and PGS grafts. By 12 weeks, only a few cells in the grafts were positively stained with CD206 or iNOS, indicating a reduced macrophage infiltration and resolution of inflammation (Fig. 5e and f).

3.5 Endothelial cell (EC) coverage and SMC distribution

EC coverage on the luminal surface of the vascular grafts were examined with both immunohistochemical and immunofluorescent staining using EC specific markers VWF and endothelial nitric oxide synthase (eNOS), respectively. As shown in Fig. 6a and Supplementary Fig. 6, the luminal surface was positively stained with VWF and eNOS for all the three types of vascular grafts in week 4, indicating a good EC coverage. The same results were observed in the explants in week 12 (Fig. 6c). These results demonstrate that all three types of grafts could be endothelialized within 4 weeks and maintain the endothelium for at least 12 weeks.

We also stained mid-sections of grafts with calponin and alpha-smooth muscle actin (αSMA) to characterize the distribution of smooth muscle cells (SMCs). The calponin$^+$ and αSMA$^+$ cells were distributed in the same region of the remodeled grafts (Fig. 6b and d). Interestingly, the 16-PPGS grafts showed a layered distribution of calponin$^+$ and αSMA$^+$ cells on week 4, with the double positive cells present not only in the sub-luminal space but also in the adventitia separated by a band of cells that were double negative for αSMA and calponin. However, most of the double positive cells appeared only in the adventitial space of the remodeled 9-PPGS and PGS grafts (Fig. 6b). In week 12, the cells became more circumferentially aligned in all three groups and the above differences in distribution remained (Fig. 6d). These results indicate that SMC distribution is affected by the degradation rate of the elastomer core during the observation window.

3.6 ECM protein distribution

All three types of grafts showed no calcification in both week 4 and 12 (Supplementary Fig. 7), which is consistent with our previous study [29]. ECM protein deposition in the remodeled grafts was examined by histochemical and immunofluorescence staining (Fig. 7). For 16-PPGS grafts in week 4, Masson's trichrome staining showed dense collagen fibers in the inner layers and loose collagen fiber in the adventitial space. Verhoeff's elastin staining showed a dense layer of elastin in the sub-luminal space. Picro-sirius red staining revealed thick fibers with red birefringence and thin ones with green birefringence but couldn't show elastin. Thus, a black band were observed in the sub-luminal space. In addition, PCL sheaths had a distinct blue birefringence in Picro-sirius red staining under polarized light (Supplementary Fig. 4). The blue birefringence showed that the PCL sheaths located in the adventitial space. Collagen III and elastin were positively stained in both sub-luminal and adventitial spaces. However, collagen I was positively stained only in the adventitial spaces of 16-PPGS grafts (Fig. 7a). This result suggests that the phenotypes of cells in the inner layers and outer layers are different, even though both cells were positively stained by calponin and αSMA (Fig. 6b). For 9-PPGS and PGS grafts in week 4, Masson's trichrome and Verhoeff's elastin staining revealed collagen and elastin were distributed throughout the

graft walls. Picro-sirius red staining showed the blue birefringence of PCL sheaths close to lumen, unlike its location in the remodeled 16-PPGS grafts. Besides, collagen I, collagen III and elastin were all transmurally distributed as shown by immunofluorescence staining (Fig. 7a). With the proceeding of vascular remodeling, elastin and collagen III still showed a layered distribution pattern for 16-PPGS grafts by week 12, although the inner layers became thinner. In contrast, collagen I, elastin and collagen III in 9-PPGS and PGS grafts remained spread out over the whole graft walls.

3.7 Mechanical properties

Quantities of collagen and elastin were measured in this study. Biochemical assays indicated that there was no significant difference in collagen content between different types of grafts (Fig. 8a). However, elastin content in 16-PPGS grafts was significantly higher than 9-PPGS and PGS grafts. The elastin content between 9-PPGS and PGS grafts was not significantly different (Fig. 8b). Since mechanical property of vessels was determined by ECM proteins, mainly collagen and elastin, these results imply an improved mechanical property for 16-PPGS grafts.

The mechanical properties of different types of grafts were evaluated using an inflation test. The performance of 9-PPGS and PGS grafts was quite similar and an increase in pressure resulted in a limited increase in circumferential stretch (Fig. 8c). In contrast, the remodeled 16-PPGS grafts displayed a more compliant nature. The circumferential stretch of 16-PPGS grafts increased with an increase in pressure from 0–60 mmHg, which was close to the native carotid arteries. The change in circumferential stretch was more limited when the pressure was above 60 mmHg (Fig. 8c). Overall, the compliance of 16-PPGS grafts was higher than 9-PPGS grafts, while PGS grafts had a lower compliance than 9-PPGS grafts (Fig. 8d). However, there was no significant difference in burst pressure, a marker of bulk strength, between the three different types of grafts (Fig. 8e).

4. Discussions

In this study, we modified PGS with palmitic acid to slow down its degradation. The palmitate substitution of PGS increases its hydrophobicity (Fig. 1c) and leads to a slower degradation *in vitro* (Fig. 1d). It is likely that the higher hydrophobicity of PPGS leads to less infiltration of circulating cells in PPGS grafts than pure PGS grafts, which also contributes to a slower degradation of PPGS grafts post-implantation (Fig. 3a). Porous PGS has been shown to almost completely degrade within 2 weeks in a mouse subcutaneous implantation model [34]. Besides, we would like to note that the PGS in this study was sourced commercially and have an even faster degradation rate than PGS in our previous studies. Because of a slower degradation of 16-PPGS, the core of 16-PPGS grafts shall provide a more stable substrate for host cells to adhere and synthesize ECM. As a result, the inner diameter of 16-PPGS grafts is closer to origin and smaller than PGS grafts in week 2 (Fig. 2c). In addition, the location of PCL sheath in the remodeled grafts are consistent with a slower degradation of 16-PPGS. PCL is the sheath material of grafts (Supplementary Fig. 3 and 4). PCL appeared in the outer layers of 16-PPGS grafts in week 4, while it was closer to the lumen of PGS and 9-PPGS grafts (Fig. 3b and Picrosiruis red staining in Fig. 7a). This

indicates that the space corresponding to16-PPGS core is still there, which is already highly cellularized and deposited with a substantial amount of ECM, while PGS and 9-PPGS cores have almost completely degraded by week 4, bringing the PCL sheaths close to lumen. Furthermore, the inner layer of unstained 16-PPGS graft samples showed a small patch of material residuals as well as some fibril-like remnants in week 4, which disappeared in week 12 (Supplementary Fig. 5). Meanwhile, PCL layers in PGS and 9-PPGS grafts were much thinner than PCL layers in 16-PPGS grafts in week 12 (Fig.3). Fast degradation of PGS or 9-PPGS could expose PCL layers to blood flow faster than slow degrading 16-PPGS. Due to higher mass transfer, the PCL layers in PGS and 9-PPGS grafts degrades faster and becomes thinner. All these results are consistent with the notion that 16-PPGS degrades more slowly than PGS and leaves a layer of autologous tissue behind in its place.

The patency of grafts in PGS group was 69.2% (9 out of 13 rats) in this study, which was lower than our previously reported patency of a similar PGS grafts (90.5%, 19 out of 21 rats) [29]. The PGS used to make grafts in this study was provided by Secant Group, LLC, whereas our previous study used PGS prepared in house [29]. The latter had significantly higher molecular weight and likely contributed to the difference in patency and host response of the PGS grafts. However, the trend of impact of degradation rate on host response should hold true as all polymers synthesized or directly used in this study were based on the same lot of commercial PGS. Another possible reason for the different patency is that the sample size (13 rats) in this study was smaller than the previous one (21 rats) [29]. The patency for PGS groups shall be further increased if more rats were used.

Slow degrading PPGS may favor graft remodeling though reducing over-proliferation of cells that surround grafts. To our PCL-PGS composite grafts, PGS layers would provide the initial mechanical strength of the grafts. When PGS layers completely degrade, PCL layers alone will dilate under blood pressure due to lack of elasticity. As compensation, the cells surrounding grafts would over proliferate to maintain mechanical strength of graft walls. This is probably the reason for a thick layer of SMC-like cells surrounding 9-PPGS and PGS grafts (Fig 4a and b). Folding and shrinking of PCL layers in PGS and 9-PPGS grafts is probably due to the push by these over-proliferated cells. Meanwhile, 16-PPGS degraded more slowly (Fig. 1d) and could provide mechanical strength to the grafts longer. In this case, there is no need for cells to over proliferate to support the load-bearing of the grafts. As such, there was only a thin layer of cells surrounding the grafts, as well as less folding and shrinking of the PCL layers (Fig 4a and b).

The slower degradation of PPGS could also dampen the acute inflammatory response associated with the degradation products of synthetic materials. Inflammation may alter the phenotype of normal SMCs [35] and make them have some characteristics of fibroblasts [36]. Indeed, the SMCs in the outer layers of PGS and 9-PPGS grafts over proliferated and highly expressed collagen I (Fig. 4 and 7). In contrast, the inner layer of 16-PPGS grafts were highly cellularized and the inflammation were milder and only limited to the adventitial spaces (Fig. 3–5). The cells in the inner layer of 16-PPGS grafts are likely to be bone marrow-derived circulating monocytes. There is certain evidence, although currently debated, that the monocytes can differentiate into SMCs, which are reported to be involved in vascular graft remodeling [37, 38]. A slower degrading PGS derivative may help

accommodate these cells and meanwhile block the infiltration of inflammatory cells from the adventitial space. Consequently, SMCs in the inner layer of 16-PPGS grafts expressed higher amount of collagen III and elastin but little collagen I, (Fig. 7), resembling the media of a native artery.

Finally, a slow degradation of PPGS may enable a layered distribution of ECM proteins. The inner layer of 16-PPGS grafts deposited with elastin and collagen III but no collagen I, while the outer layer accumulated with collagen III, elastin and collagen I, the same ECM composition as what was distributed throughout the walls of 9-PPGS and PGS grafts (Fig. 7). Such a layered distribution of ECM proteins probably contributes to the closer resemblance of the mechanical property between 16-PPGS grafts and the native arteries (Fig. 8c–e). In native carotid arteries, elastin and collagen III dominate the ECM in the media, while collagen I is mainly distributed in the adventitia (Fig. 7). When blood pressure is in a normal range, elastin stretches and makes vessels elastic. On the other hand, when blood pressure is abnormally high, collagen I takes over the leading role in loadbearing and maintains vessel integrity [39, 40]. However, when elastin and collagen I are deposited together, it is possible that elastin cannot be fully stretched. The mechanical properties of collagen I make vessels become stiff. Mechanical properties displayed by PGS and 9-PPGS grafts are likely results of the presence of both elastin and collagen I throughout the graft walls. Therefore, 16-PPGS grafts showed a superior mechanical property as compared to PGS and 9-PPGS grafts (Fig. 8c–e).

There are some limitations of this study that need to be addressed in the future experiments. First, the possible release of palmitic acid from PPGS *in vivo* is not evaluated in this study. Palmitic acid is the most abundant saturated fatty acid in our bodies [41]. However, an elevated palmitate level can cause inflammation [42, 43]. Because the degradation of PPGS is slow, we believe the concentration of palmitic acid in the grafts would be low. In fact, inflammation was mild in the inner layer of 16-PPGS grafts (Fig. 5). Second, the effect of mechanical properties of grafts on MSCs is not investigated in this study. The mechanical properties of three different types of grafts were different prior to implantation (Fig. 1f–i). 16-PPGS grafts were softer than the other two types of grafts. Since vascular smooth muscle cells have been reported to function differently on substrates with different moduli [44], it is possible that a softer graft wall also contributes to the improved performance of 16-PPGS grafts *in vivo*. Third, PPGS and PGS are chemically different. However, we don't believe the palmitate modification would make PGS bioactive. In fact, it is difficult to alter degradation profile of one material without changing its chemical structure. Lastly, the observation window of this study is only 3-month. A longer-term study will reveal how the conduit behaves after complete degradation of graft materials.

5. Conclusions

In this study, we modified PGS with palmitic acid to slow down its degradation. Vascular grafts made of PPGS were more hydrophobic and degraded more slowly *in vitro*. When implanted into rat common carotid arteries, 16-PPGS grafts had a higher patency, a layered distribution of SMCs and ECM proteins resembling native arteries more closely. Furthermore, 16-PPGS grafts induced less inflammation and exhibited a more robust

mechanical property as compared to 9-PPGS and PGS grafts. These results indicated that slow degrading PGS derivatives improved the overall performance of PGS-based vascular grafts.

Supplementary Material

Refer to Web version on PubMed Central for supplementary material.

Acknowledgements:

This project is supported by NIH R01HL089658, S10OD016191, S10OD025049 and DOD PR181709.

7. Reference

[1]. Edelman ER, Vascular tissue engineering : designer arteries, Circ Res85(12) (1999) 1115–7. [PubMed: 10590236]

[2]. Gaudino M, Rahouma M, Abouarab A, Leonard J, Kamel M, Di Franco A, Demetres M, Tam DY, Tranbaugh R, Girardi LN, Fremes SE, Radial artery versus saphenous vein as the second conduit for coronary artery bypass surgery: A meta-analysis, J Thorac Cardiov Sur157(5) (2019) 1819-+.

[3]. Gaudino M, Lorusso R, Rahouma M, Abouarab A, Tam DY, Spadaccio C, Saint-Hilary G, Leonard J, Iannaccone M, D'Ascenzo F, Di Franco A, Soletti G, Kamel MK, Lau C, Girardi LN, Schwann TA, Benedetto U, Taggart DP, Fremes SE, Radial Artery Versus Right Internal Thoracic Artery Versus Saphenous Vein as the Second Conduit for Coronary Artery Bypass Surgery: A Network Meta-Analysis of Clinical Outcomes, J Am Heart Assoc8(2) (2019).

[4]. Athanasiou T, Saso S, Rao C, Vecht J, Grapsa J, Dunning J, Lemma M, Casula R, Radial artery versus saphenous vein conduits for coronary artery bypass surgery: forty years of competition - which conduit offers better patency? A systematic review and meta-analysis, Eur J Cardio-Thorac40(1) (2011) 208–220.

[5]. Lord RS, Nash PA, Raj BT, Stary DL, Graham AR, Hill DA, Tracy GD, Goh KH, Prospective randomized trial of polytetrafluoroethylene and Dacron aortic prosthesis. I. Perioperative results, Ann Vasc Surg2(3) (1988) 248–54. [PubMed: 2973343]

[6]. Friedman SG, Lazzaro RS, Spier LN, Moccio C, Tortolani AJ, A prospective randomized comparison of Dacron and polytetrafluoroethylene aortic bifurcation grafts, Surgery117(1) (1995) 7–10. [PubMed: 7809840]

[7]. Klinkert P, Post PN, Breslau PJ, van Bockel JH, Saphenous vein versus PTFE for above-knee femoropopliteal bypass. A review of the literature, Eur J Vasc Endovasc Surg27(4) (2004) 357–62. [PubMed: 15015183]

[8]. Wang X, Lin P, Yao Q, Chen C, Development of small-diameter vascular grafts, World J Surg31(4) (2007) 682–9. [PubMed: 17345123]

[9]. Soletti L, Hong Y, Guan JJ, Stankus JJ, El-Kurdi MS, Wagner WR, Vorp DA, A bilayered elastomeric scaffold for tissue engineering of small diameter vascular grafts, Acta Biomaterialia6(1) (2010) 110–122. [PubMed: 19540370]

[10]. Zhou M, Liu Z, Liu C, Jiang X, Wei Z, Qiao W, Ran F, Wang W, Qiao T, Liu C, Tissue engineering of small-diameter vascular grafts by endothelial progenitor cells seeding heparin-coated decellularized scaffolds, J Biomed Mater Res B Appl Biomater100(1) (2012) 111–20. [PubMed: 22113845]

[11]. Cho SW, Lim SH, Kim IK, Hong YS, Kim SS, Yoo KJ, Park HY, Jang Y, Chang BC, Choi CY, Hwang KC, Kim BS, Small-diameter blood vessels engineered with bone marrow-derived cells, Ann Surg241(3) (2005) 506–15. [PubMed: 15729075]

[12]. Song Y, Feijen J, Grijpma DW, Poot AA, Tissue engineering of small-diameter vascular grafts: a literature review, Clin Hemorheol Microcirc49(1–4) (2011) 357–74. [PubMed: 22214707]

[13]. Hibino N, Shin'oka T, Matsumura G, Ikada Y, Kurosawa H, The tissue-engineered vascular graft using bone marrow without culture, J Thorac Cardiov Sur129(5) (2005) 1064–1070.

[14]. Nieponice A, Soletti L, Guan JJ, Deasy BM, Huard J, Wagner WR, Vorp DA, Development of a tissue-engineered vascular graft combining a biodegradable scaffold, muscle-derived stem cells and a rotational vacuum seeding technique, Biomaterials29(7) (2008) 825–833. [PubMed: 18035412]

[15]. Roh JD, Nelson GN, Brennan MP, Mirensky TL, Yi T, Hazlett TF, Tellides G, Sinusas AJ, Pober JS, Saltzman WM, Kyriakides TR, Breuer CK, Small-diameter biodegradable scaffolds for functional vascular tissue engineering in the mouse model, Biomaterials29(10) (2008) 1454–1463. [PubMed: 18164056]

[16]. Dahl SLM, Kypson AP, Lawson JH, Blum JL, Strader JT, Li YL, Manson RJ, Tente WE, DiBernardo L, Hensley MT, Carter R, Williams TP, Prichard HL, Dey MS, Begelman KG, Niklason LE, Readily Available Tissue-Engineered Vascular Grafts, Sci Transl Med3(68) (2011).

[17]. Lawson JH, Glickman MH, Ilzecki M, Jakimowicz T, Jaroszynski A, Peden EK, Pilgrim AJ, Prichard HL, Guziewicz M, Przywara S, Szmidt J, Turek J, Witkiewicz W, Zapotoczny N, Zubilewicz T, Niklason LE, Bioengineered human acellular vessels for dialysis access in patients with end-stage renal disease: two phase 2 single-arm trials, Lancet387(10032) (2016) 2026–2034. [PubMed: 27203778]

[18]. Kirkton RD, Santiago-Maysonet M, Lawsonl JH, Tente WE, Dahl SLM, Niklason LE, Prichard HL, Bioengineered human acellular vessels recellularize and evolve into living blood vessels after human implantation, Sci Transl Med11(485) (2019).

[19]. Brothers TE, Stanley JC, Burkel WE, Graham LM, Small-Caliber Polyurethane and Polytetrafluoroethylene Grafts - a Comparative-Study in a Canine Aortoiliac Model, J Biomed Mater Res24(6) (1990) 761–771. [PubMed: 2361967]

[20]. Tiwari A, Salacinski H, Seifalian AM, Hamilton G, New prostheses for use in bypass grafts with special emphasis on polyurethanes, Cardiovasc Surg10(3) (2002) 191–197. [PubMed: 12044423]

[21]. Seifu DG, Purnama A, Mequanint K, Mantovani D, Small-diameter vascular tissue engineering, Nat Rev Cardiol10(7) (2013) 410–21. [PubMed: 23689702]

[22]. Wang Z, Cui Y, Wang J, Yang X, Wu Y, Wang K, Gao X, Li D, Li Y, Zheng XL, Zhu Y, Kong D, Zhao Q, The effect of thick fibers and large pores of electrospun poly(epsilon-caprolactone) vascular grafts on macrophage polarization and arterial regeneration, Biomaterials35(22) (2014) 5700–10. [PubMed: 24746961]

[23]. de Valence S, Tille JC, Mugnai D, Mrowczynski W, Gurny R, Moller M, Walpoth BH, Long term performance of polycaprolactone vascular grafts in a rat abdominal aorta replacement model, Biomaterials33(1) (2012) 38–47. [PubMed: 21940044]

[24]. Filipe EC, Santos M, Hung J, Lee BSL, Yang N, Chan AHP, Ng MKC, Rnjak-Kovacina J, Wise SG, Rapid Endothelialization of Off-the-Shelf Small Diameter Silk Vascular Grafts, JACC Basic Transl Sci3(1) (2018) 38–53. [PubMed: 30062193]

[25]. Wu W, Allen RA, Wang YD, Fast-degrading elastomer enables rapid remodeling of a cell-free synthetic graft into a neoartery, Nat Med18(7) (2012) 1148-+. [PubMed: 22729285]

[26]. Lee KW, Stolz DB, Wang Y, Substantial expression of mature elastin in arterial constructs, Proc Natl Acad Sci U S A108(7) (2011) 2705–10. [PubMed: 21282618]

[27]. Crapo PM, Wang YD, Physiologic compliance in engineered small-diameter arterial constructs based on an elastomeric substrate, Biomaterials31(7) (2010) 1626–1635. [PubMed: 19962188]

[28]. Allen RA, Wu W, Yao MY, Dutta D, Duan XJ, Bachman TN, Champion HC, Stolz DB, Robertson AM, Kim K, Isenberg JS, Wang YD, Nerve regeneration and elastin formation within poly(glycerol sebacate)-based synthetic arterial grafts one-year post-implantation in a rat model, Biomaterials35(1) (2014) 165–173. [PubMed: 24119457]

[29]. Lee KW, Gade PS, Dong LW, Zhang ZX, Aral AM, Gao J, Ding XC, Stowell CET, Nisar MU, Kim K, Reinhardt DP, Solari MG, Gorantla VS, Robertson AM, Wang YD, A biodegradable synthetic graft for small arteries matches the performance of autologous vein in rat carotid arteries, Biomaterials181 (2018) 67–80. [PubMed: 30077138]

[30]. Sandwick RK, Schray KJ, The Inactivation of Enzymes Upon Interaction with a Hydrophobic Latex Surface, J Colloid Interf Sci115(1) (1987) 130–138.

[31]. Koutsopoulos S, Patzsch K, Bosker WTE, Norde W, Adsorption of trypsin on hydrophilic and hydrophobic surfaces, Langmuir23(4) (2007) 2000–2006. [PubMed: 17279687]

[32]. Borjesson J, Engqvist M, Sipos B, Tjerneld F, Effect of poly(ethylene glycol) on enzymatic hydrolysis and adsorption of cellulase enzymes to pretreated lignocellulose, Enzyme Microb Tech41(1–2) (2007) 186–195.

[33]. Ding X, Chen Y, Chao C, Wu Y-L, Wang Y, Control the mechanical properties and degradation of poly(glycerol sebacate) by substitution of the hydroxyl groups with palmitates, Macromolecular bioscience DOI:10.1002/mabi.202000101 (2020).

[34]. Ding X, Wu YL, Gao J, Wells A, Lee K, Wang Y, Tyramine functionalization of poly(glycerol sebacate) increases the elasticity of the polymer, J Mater Chem B5(30) (2017) 6097–6109. [PubMed: 29276605]

[35]. Rocnik EF, Chan BM, Pickering JG, Evidence for a role of collagen synthesis in arterial smooth muscle cell migration, J Clin Invest101(9) (1998) 1889–98. [PubMed: 9576753]

[36]. van den Borne SWM, Diez J, Blankesteijn WM, Verjans J, Hofstra L, Narula J, Myocardial remodeling after infarction: the role of myofibroblasts, Nature Reviews Cardiology7(1) (2010) 30–37. [PubMed: 19949426]

[37]. Roh JD, Sawh-Martinez R, Brennan MP, Jay SM, Devine L, Rao DA, Yi T, Mirensky TL, Nalbandian A, Udelsman B, Hibino N, Shinoka T, Saltzman WM, Snyder E, Kyriakides TR, Pober JS, Breuer CK, Tissue-engineered vascular grafts transform into mature blood vessels via an inflammation-mediated process of vascular remodeling, P Natl Acad Sci USA107(10) (2010) 4669–4674.

[38]. Talacua H, Smits AIPM, Muylaert DEP, van Rijswijk JW, Vink A, Verhaar MC, Driessen-Mol A, van Herwerden LA, Bouten CVC, Kluin J, Baaijens FPT, In Situ Tissue Engineering of Functional Small-Diameter Blood Vessels by Host Circulating Cells Only, Tissue Eng Pt A21(19–20) (2015) 2583–2594.

[39]. Fortunato RN, Robertson AM, Sang C, Maiti S, Computational modeling reveals the relationship between intrinsic failure properties and uniaxial biomechanical behavior of arterial tissue, Biomech Model Mechan18(6) (2019) 1791–1807.

[40]. Hill MR, Duan XJ, Gibson GA, Watkins S, Robertson AM, A theoretical and non-destructive experimental approach for direct inclusion of measured collagen orientation and recruitment into mechanical models of the artery wall, J Biomech45(5) (2012) 762–771. [PubMed: 22305290]

[41]. Ubhayasekera SJ, Staaf J, Forslund A, Bergsten P, Bergquist J, Free fatty acid determination in plasma by GC-MS after conversion to Weinreb amides, Anal Bioanal Chem405(6) (2013) 1929–35. [PubMed: 23307129]

[42]. Wang Y, Qian YY, Fang QL, Zhong P, Li WX, Wang LT, Fu WT, Zhang YL, Xu Z, Li XK, Liang G, Saturated palmitic acid induces myocardial inflammatory injuries through direct binding to TLR4 accessory protein MD2, Nature Communications8 (2017).

[43]. Korbecki J, Bajdak-Rusinek K, The effect of palmitic acid on inflammatory response in macrophages: an overview of molecular mechanisms, Inflamm Res68(11) (2019) 915–932. [PubMed: 31363792]

[44]. Steucke KE, Tracy PV, Hald ES, Hall JL, Alford PW, Vascular smooth muscle cell functional contractility depends on extracellular mechanical properties, J Biomech48(12) (2015) 3044–3051. [PubMed: 26283412]

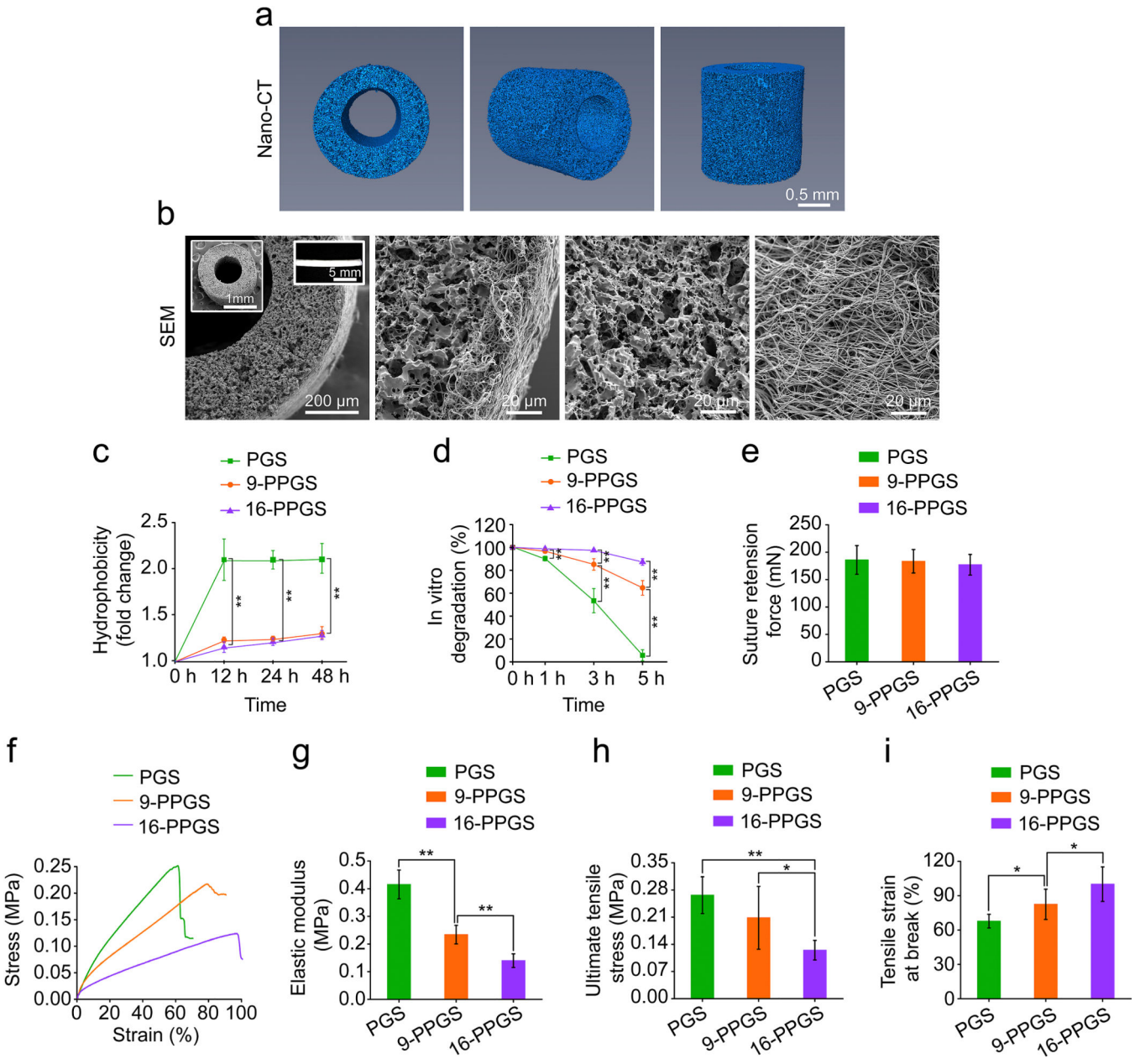

Fig. 1.

(a) Reconstructed 3D images of nano-CT scanning of grafts. (b) SEM images of grafts. Insets: low magnification SEM images of the graft (left) and macroscopic view of the graft (right). (c) Hydrophobicity of three different types of grafts. (d) *In vitro* degradation of three different types of grafts. (e) Suture retention forces of three different types of grafts. (f) Representative stress-strain curves of three different types of grafts. (g) Elastic modulus of three different types of grafts. (h) Ultimate tensile stress of three different types of grafts. (i) Tensile strain at break of three different types of grafts. * indicates $p < 0.05$, compared between two groups; ** indicates $p < 0.01$, compared between two groups.

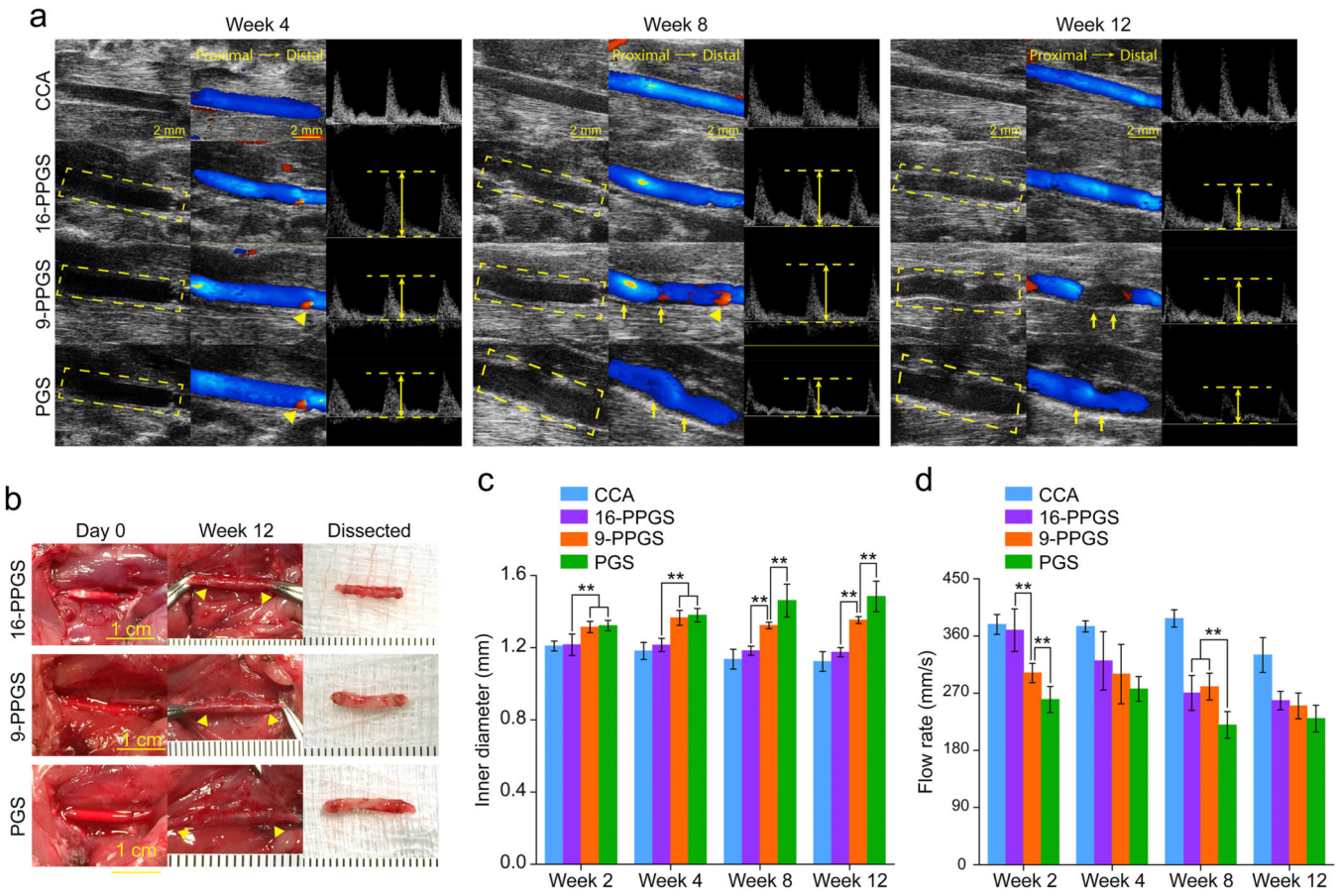

Fig. 2.

(a) Ultrasound images of three different types of grafts implanted into rat common carotid arteries. Left column: B mode; Middle column: color mode; Right column: PW mode. Dash squares indicate the implanted grafts. The height of double arrows indicates the rate of peak flow. Arrow heads indicate back flow of blood. Arrows indicate distortion of grafts. (b) Macroscopic views of three different types of grafts upon implantation and 12 weeks post-operation. Arrow heads indicate anastomosis sites. (c) Inner diameter of three different types of grafts 12 weeks post-implantation. (d) Peak rate of blood flow of three different types of grafts 12 weeks post-implantation. ** indicates $p < 0.01$, compared between two groups.

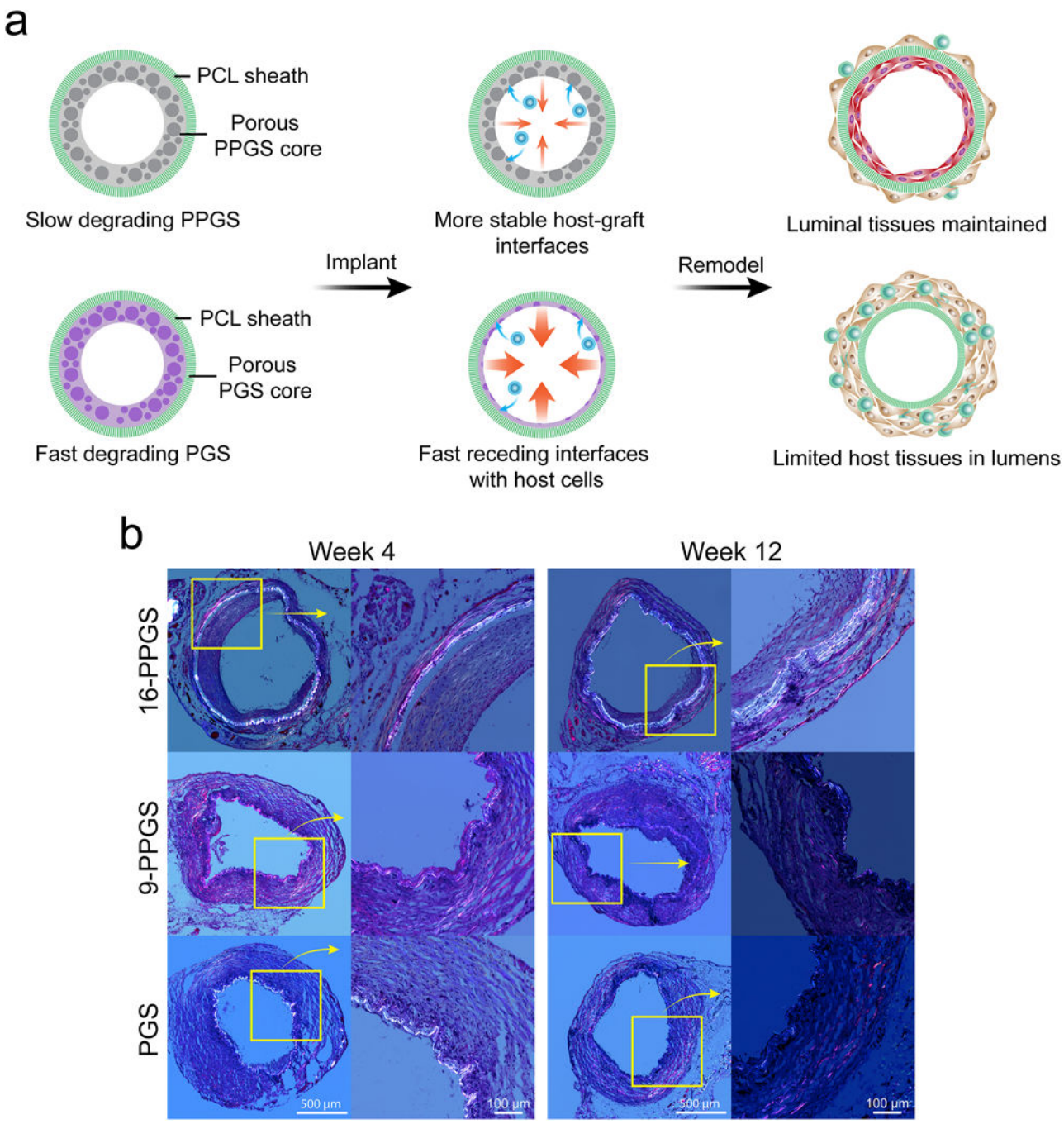

Fig. 3.

(a) The impact of degradation rate of PGS and its derivative derivatives on host remodeling of vascular grafts. PGS is less hydrophobic and degrades fast *in vivo*. The PGS graft presents a less stable and relatively fast receding interface with host cells. This could explain why the graft dilates. PPGS is more hydrophobic and degrades slower *in vivo*. The more stable interface leads to the maintenance of the luminal tissues. Here we use commercially available PGS (Regenerez®) that has a lower molecular weight and degrades faster than

PGS used in our previous studies that is synthesized in house [29]. (b) H&E staining of three different types of grafts explanted in week 4 and 12 under polarized light.

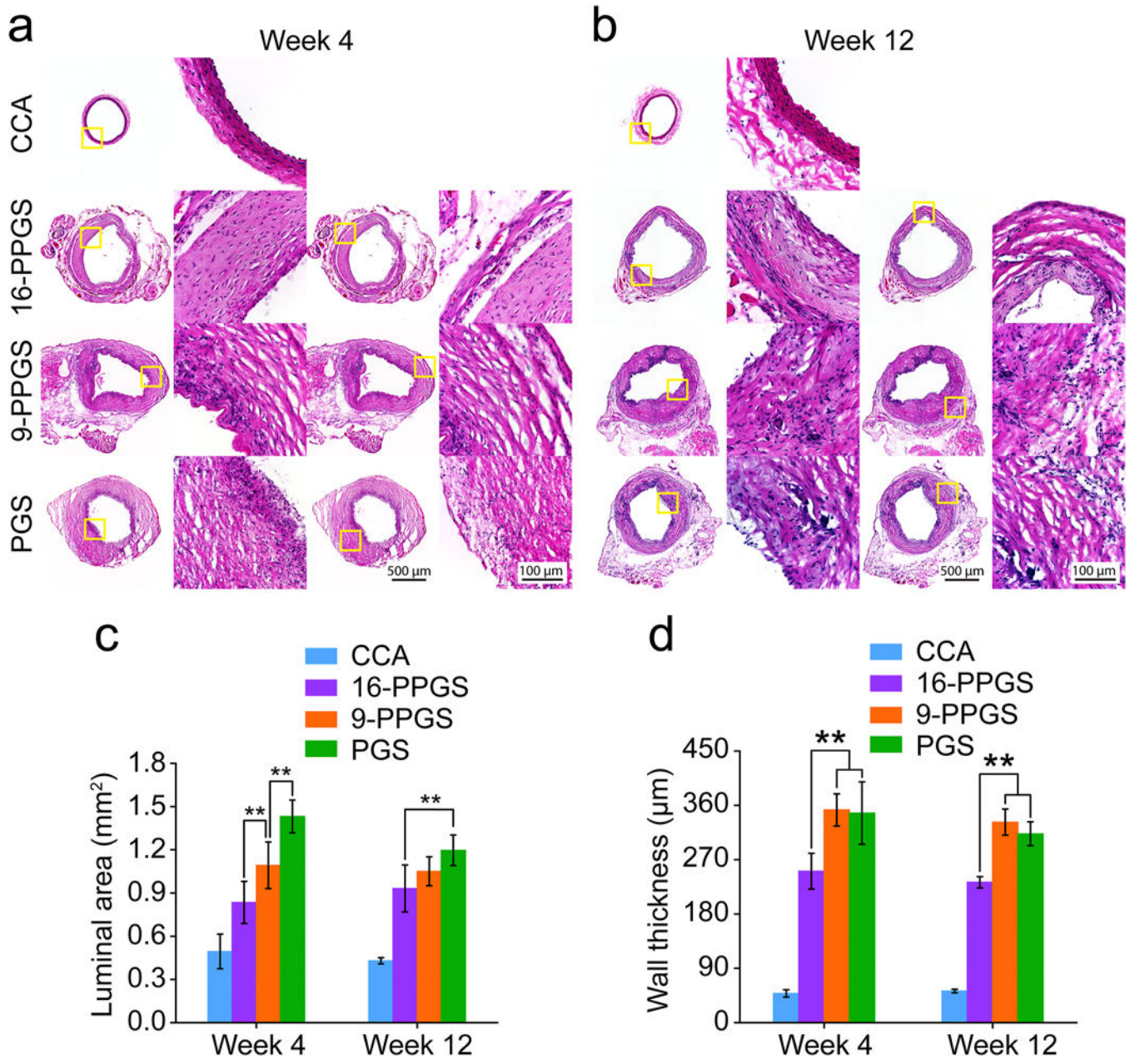

Fig. 4.

(a) H&E staining of three different types of grafts explanted in week 4. (b) H&E staining of three different types of grafts explanted in week 12. (c) Quantification of luminal areas of three different types of grafts explanted in week 4 and 12. (d) Quantification of graft wall thickness of three different types of grafts explanted in week 4 and 12. ** indicates $p < 0.01$, compared between two groups.

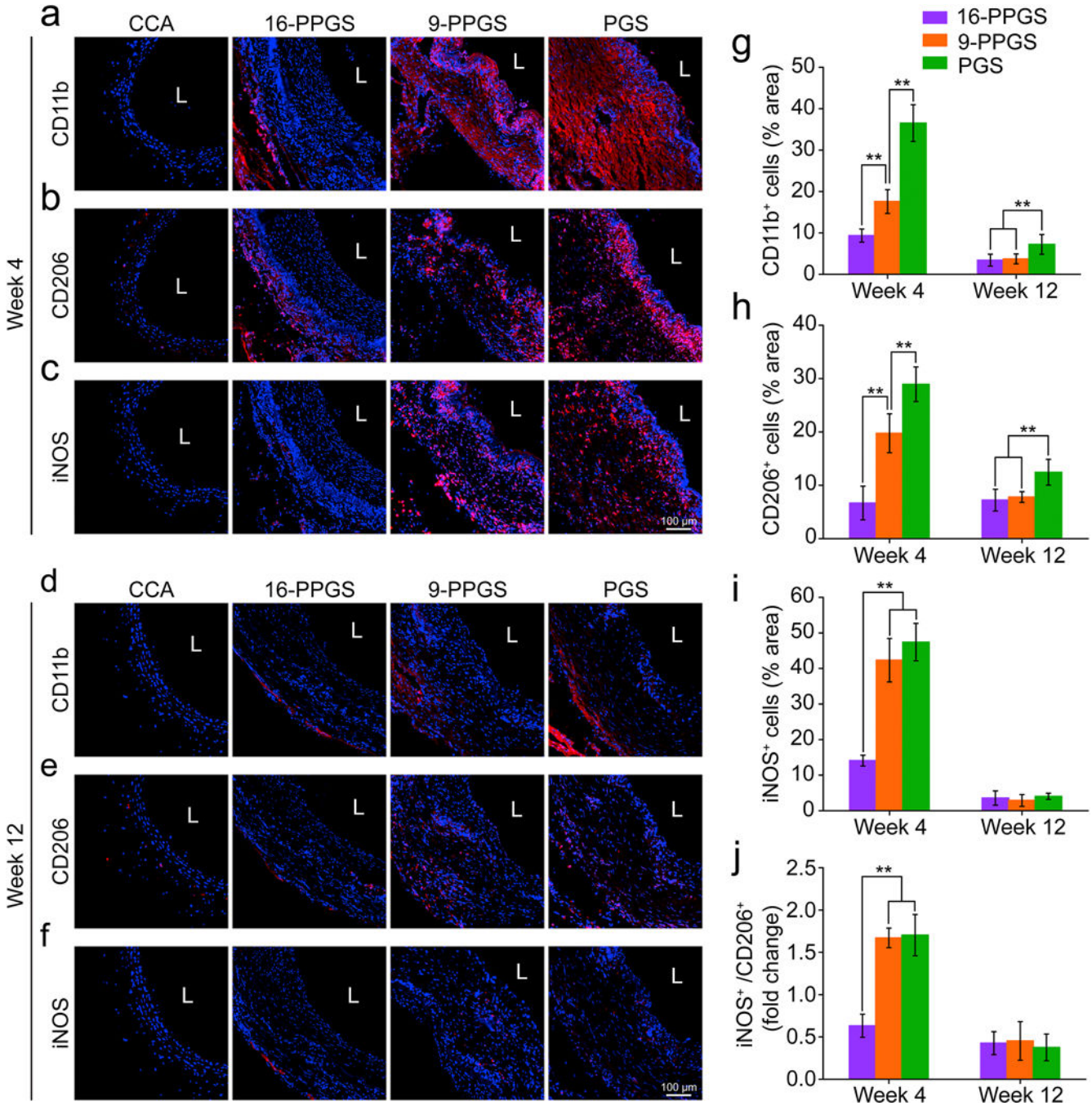

Fig. 5.

(a-c) Immunofluorescence staining of CD11b, CD206 and iNOS in three different types of grafts in week 4. (d-f) Immunofluorescence staining of CD11b, CD206 and iNOS in three different types of grafts in week 12. Blue colors indicate nucleus and red colors indicate positive staining. L indicates lumen. (g) Quantification of $CD11b^+$ cells in three different types of grafts in week 4 and 12. (h) Quantification of $CD206^+$ cells in three different types of grafts in week 4 and 12. (i) Quantification of $iNOS^+$ cells in three different types of grafts

in week 4 and 12. (j) Quantification of ratio of $iNOS^+$ cells/$CD206^+$ cells in three different types of grafts in week 4 and 12. ** indicates $p < 0.01$, compared between two groups.

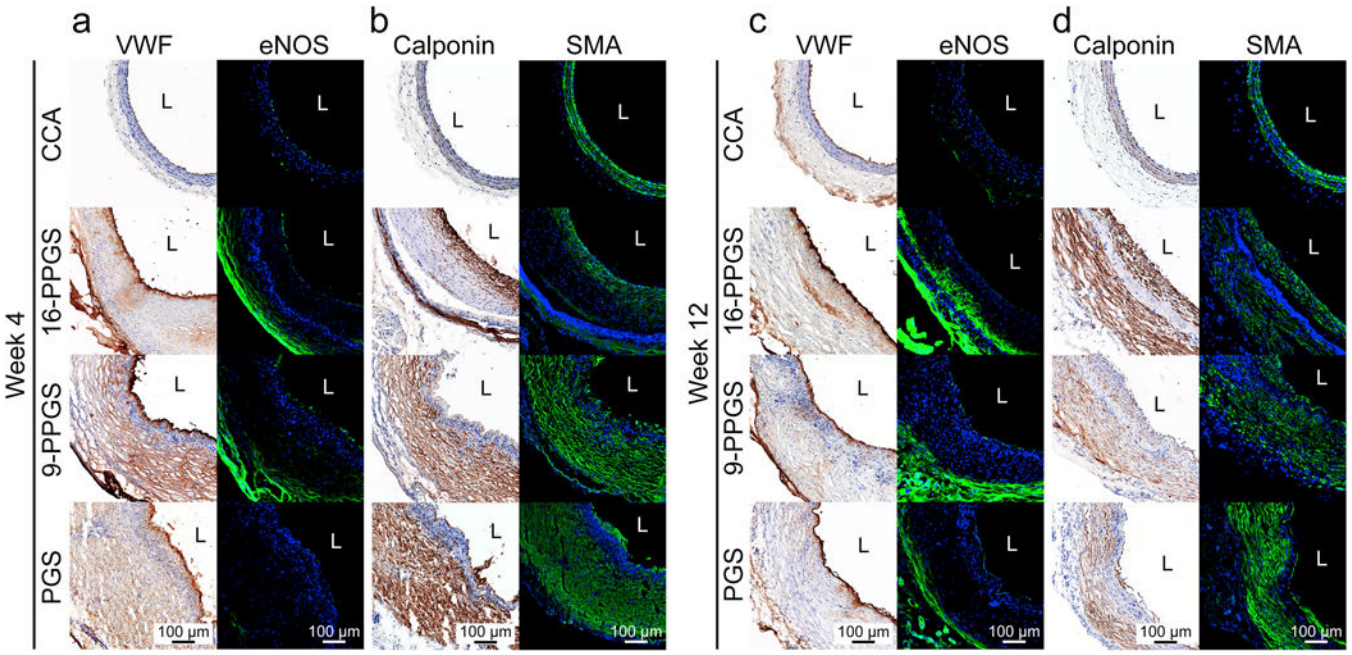

Fig. 6.

(a) Immunohistochemical staining of VWF and immunofluorescence staining of eNOS in three different types of grafts in week 4. (b) Immunohistochemical staining of calponin and SMA in three different types of grafts in week 4. (c) Immunohistochemical staining of VWF and immunofluorescence staining of eNOS in three different types of grafts in week 12. (d) Immunohistochemical staining of calponin and SMA in three different types of grafts in week 12. Blue colors indicate nucleus, and green colors indicate positive staining. L indicates lumen.

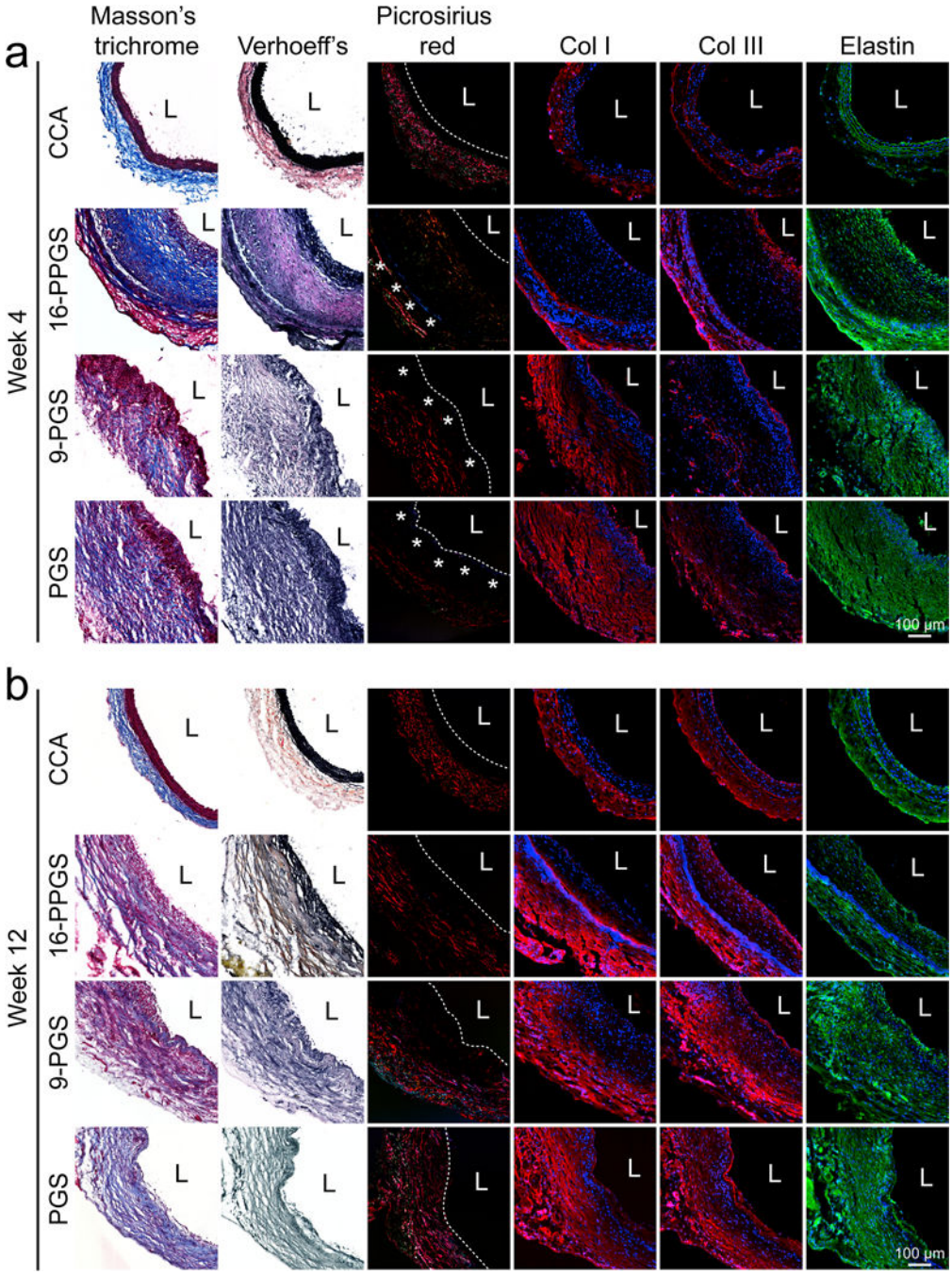

Fig. 7.

(a) Histochemical staining of Masson's trichrome, Verhoeff elastin, and Picro-sirius red, and immunofluorescence staining of collagen I, collagen III and elastin in three different types of grafts in week 4. (b) Histochemical staining of Masson's trichrome, Verhoeff elastin, and Picro-sirius red, and immunofluorescence staining of collagen I, collagen III and elastin in three different types of grafts in week 12. Blue colors indicate nucleus, and red or green colors indicate positive staining. L indicates lumen. Dash lines and asterisks in Picro-sirius

red staining indicate boundaries of lumen and specific blue birefringence shown by PCL sheaths, respectively.

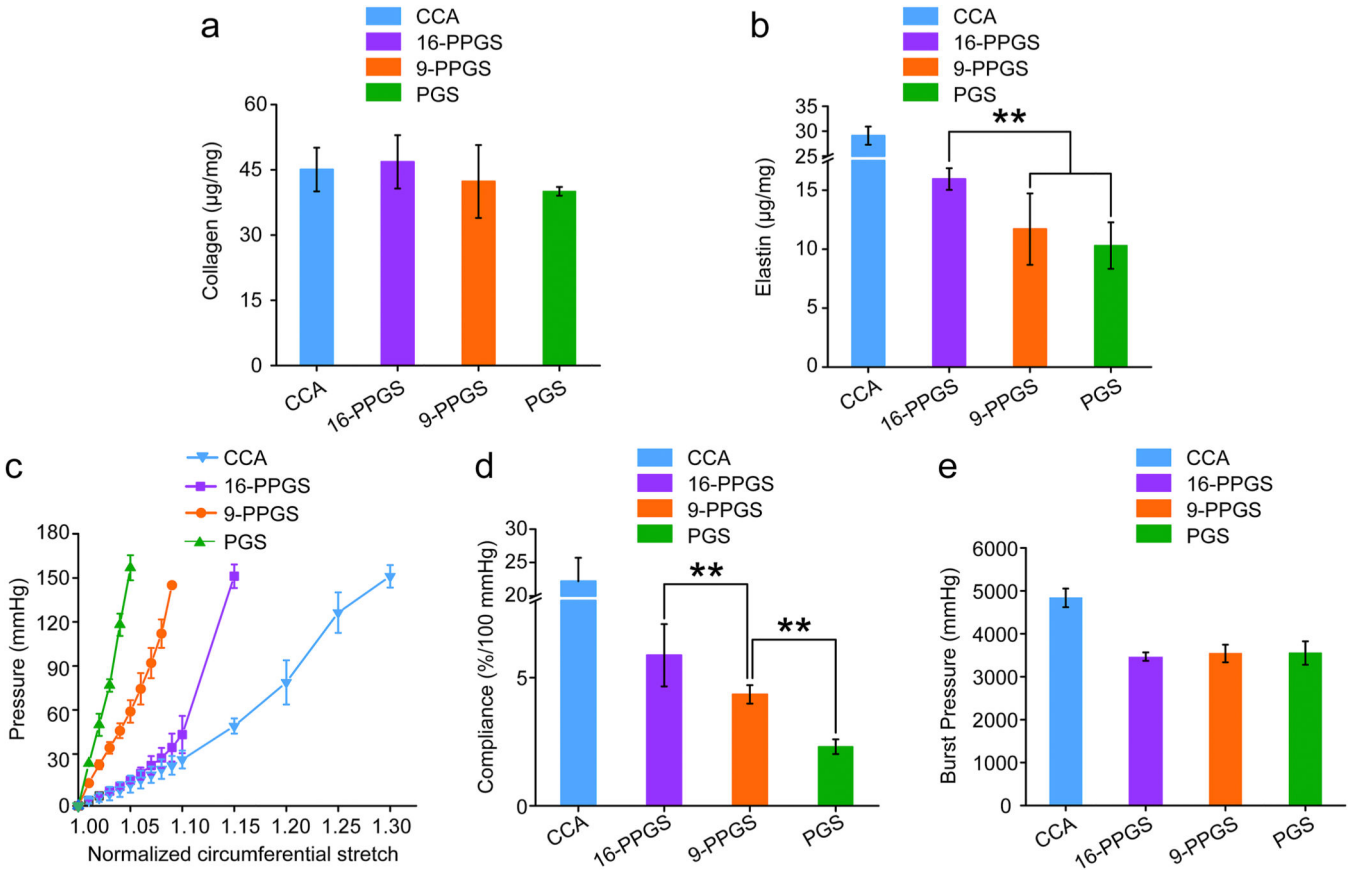

Fig. 8.

(a) Quantification of total collagen in three different types of grafts explanted in week 12. (b) Quantification of elastin in three different types of grafts explanted in week 12. (c) Circumferential pressure-stretch curves of three different types of grafts explanted in week 12. (d) Compliance of three different types of grafts explanted in week 12. (e) Burst pressure of three different types of grafts explanted in week 12. ** indicates $p < 0.01$, compared between two groups.

Table 1.

Patency of three different types of grafts.

Group	Number	Patency	
		Week2	Week4
16-PPGS	14	92.8% (13/14)	92.8% (13/14)
9-PPGS	12	75% (9/12)	75% (9/12)
PGS	13	69.2% (9/13)	69.2% (9/13)